A high-pressure structural study of propionic acid and the application of CCD detectors in high-pressure single-crystal x-ray diffraction

2000 J. Phys.: Condens. Matter 12 L613

(http://iopscience.iop.org/0953-8984/12/39/101)

J. Phys.: Condens. Matter **12** (2000) L613–L618. Printed in the UK PII: S0953-8984(00)16106-5

LETTER TO THE EDITOR

A high-pressure structural study of propionic acid and the application of CCD detectors in high-pressure single-crystal x-ray diffraction

David R Allan†, Stewart J Clark‡, Simon Parsons§ and Michael Ruf‖

† Department of Physics and Astronomy, The University of Edinburgh, Mayfield Road, Edinburgh, EH9 3JZ, UK
‡ Department of Physics, Durham University, Science Laboratories, South Road, Durham, DH1 3LE, UK
§ Department of Chemistry, The University of Edinburgh, Edinburgh, EH9 3JJ, UK
‖ Bruker AXS GmbH, Advanced X-ray Systems, 76181 Karlsruhe, Germany¶

Received 4 August 2000

Abstract. We have determined the high-pressure crystal-structure of propionic acid, including the calculated positions of the hydrogen atoms, using a combination of single-crystal x-ray diffraction techniques and *ab initio* density functional calculations. We find that a previously unobserved triclinic $P\bar{1}$ high-pressure phase and the low-temperature monoclinic $P2_1/c$ phase are both stable over a narrow pressure range just above the ambient temperature crystallization pressure. Both structures are characterized by the formation of isolated dimers and our calculations indicate that the rearrangement of the molecules between the two structures results in a very small reduction in the enthalpy (0.062 eV/molecule) for the triclinic phase. The high-pressure single-crystal x-ray diffraction work was partly undertaken on a diffractometer equipped with a CCD detector. We outline the techniques required for such studies and the considerable improvement in data quality that can be gained.

Propionic acid (CH_3CH_2COOH) is the first in the series of saturated monocarboxylic acids to form a crystalline phase at low-temperature characterized by the formation of isolated dimer pairs of molecules linked by hydrogen bonding, even though this is by far the most common intermolecular bonding motif for carboxylic acids. The smaller molecules in the series, formic acid (HCOOH) and acetic acid (CH_3COOH), distinguish themselves by forming crystal structures at low temperature with infinite hydrogen-bonded molecular chains rather than dimers. Both formic acid and acetic acid crystallize in the $Pna2_1$ space group at temperatures of 8 °C and 16 °C respectively with remarkably similar conformations of the carboxyl groups within the chains—the structures being essentially identical with the exception of the methyl group in acetic acid.

In our recent study of the high-pressure phase of formic acid [1] we found that the molecules also form infinite hydrogen bonded chains although they adopt both the *cis* and *trans* conformers rather than only the *trans* form of the low-temperature phase. The molecules are arranged in pairs on symmetrically flat layers so that 'near dimers' are created between adjacent molecules in the same chain—though the required bond lengths for 'true dimer' formation are significantly shorter than those observed. For acetic acid, we find that, despite the low-freezing pressure of only 0.2 GPa, the high-pressure crystal structure is quite different from that formed at low temperature [2]. Although the hydrogen-bonded molecular chains of the high-pressure structure

¶ Present address.

0953-8984/00/390613+06$30.00

are virtually identical to those of the low-temperature phase, the relative orientations of the chains are markedly different. The chains re-orient in such a manner that puckered molecular layers are formed, providing a more efficient molecular packing, and so that a substantially different methyl-methyl contact motif is created between adjacent molecular chains.

For both formic acid and acetic acid, then, we find that the high-pressure structures retain the infinite hydrogen bonded chains of the low-temperature forms—although for formic acid there is a potential route to dimer formation. Here we report the first high-pressure structural study of propionic acid which, as already stated, is the first member of the saturated monocarboxylic acid series to form a crystal structure composed of dimers. We find that the low-temperature monoclinic $P2_1/c$ phase and a previously unobserved triclinic $P\bar{1}$ high-pressure phase are both stable over the limited range of pressure covered in this study. As for the monoclinic phase, the structure of the triclinic phase is also characterized by the formation of isolated dimers. However, these dimer pairs of molecules arrange themselves in a markedly different packing motif from the monoclinic form and results in two different classes of dimers: those with a point of inversion at their centres and those with an inversion centre at the midpoint between the dimers. A series of *ab initio* calculations indicates that this rearrangement of the molecules results in a very small reduction in the enthalpy (0.062 eV/molecule) for the triclinic structure and may explain why the monoclinic and triclinic phases can occur in the same narrow pressure range just above the ambient temperature crystallization pressure.

Liquid propionic acid was loaded and pressurized in a Merrill–Bassett diamond-anvil cell [3] which had been equipped with 600 μm culet diamonds and a tungsten gasket. After the nucleation of many crystallites the temperature was cycled close to the melting curve, in order to reduce the number of crystallites, in a manner similar to [4]. Finally, a single crystal was obtained at approximately 1.4 GPa that entirely filled the 250 μm gasket hole.

The setting angles of 25 strong reflections were determined on an Enraf–Nonius CAD4 diffractometer (equipped with a Mo x-ray tube) and a least-squares fit gave the triclinic unit-cell parameters to be $a = 7.4100(11)$ Å, $b = 7.538(2)$ Å, $c = 13.899(4)$ Å, $\alpha = 101.90(3)^\circ$, $\beta = 103.63(2)^\circ$ and $\gamma = 99.270(18)^\circ$ with a volume $V = 720.1(4)$ Å^3. This unit cell can be transformed to a metrically monoclinic C-centred cell, although the Laue symmetry of the data set is $\bar{1}$. Comparing the unit-cell volume of the high-pressure phase with that of the low-temperature phase [5], we expect there to be eight molecules in the unit cell.

Intensity data were collected with the ω-scan method at the position of least attenuation of the pressure cell, according to the fixed-ϕ technique [6]. All accessible reflections were measured in the shell $+h, \pm k, \pm l$ for 0 Å$^{-1} < \sin\theta/\lambda < 0.71$ Å^{-1}. The intensities were corrected for absorption and then used for an attempted structure solution by direct methods. However, due to the apparent complexity of the structure and the restrictions of the pressure cell limiting the accessible regions of reciprocal space, a reliable solution could not be obtained from this single set of data. Consequently, the sample was remelted and a second crystal grown with an orientation orthogonal to the first—this was achieved by selecting a nucleation point for crystal growth on the edge of the gasket and not, as for the previous crystal, on the diamond culet. An identical data collection strategy and data reduction procedure was adopted as before and the two resulting data sets were merged for final structure solution and refinement. The structure was solved by direct methods in P1, and the model then transformed to $P\bar{1}$ after identification of the inversion centres. This was undertaken with the Shelx suite of programs [7]. The final fit gave $R1 = 18.68\%$ for 547 unique data with $F > 4\sigma(F)$ and $a\ wR2 = 32.04\%$ based on F^2 and all 1558, $2\theta < 50^\circ$, data used for refinement. The goodness-of-fit was 1.662.

Given the relatively poor refinement statistics, a further data collection was performed using the Bruker P4 diffractometer equiped with the Bruker SMART 1000 CCD detector (and

a monochromated Mo sealed-tube source) as it was anticipated that the area detector would provide a substantial improvement in the precision of the measured intensities. The SMART program was used for data collection control and, with a detector to crystal distance of 60 mm, 2θ was set at -27° while ω was scanned over the range -40° to 52.8° at χ intervals of 30° from 0° to -180°. This strategy allowed the measurement of reflection intensities covering approximately 32% of the Ewald sphere to a resolution of 0.9 Å with a combination of seven sets of exposures (frames). Each frame covered a range of 0.3° in ω with ϕ fixed at 270°. A total of 1250 frames were collected with an exposure time of 30 seconds per frame. The overall data collection time was 12 h. With the SMART and RLATT code, three orientation matrices were obtained: one for the sample and two for the diamond anvils. Data integration and global cell refinement were performed with the program SAINT and three independent hkl data sets were obtained, with each affected by reflection overlap from the two other sets. The GEMINI program suite was finally used to produce an hkl intensity file containing only non-overlapping propionic acid reflections.

Existing integration packages are unable to allow for shading of the detector by the pressure cell, and a shading correction was performed in the following manner. We follow Busing and Levy in defining three co-ordinate systems: the reciprocal axis system of the crystal, the fixed laboratory axis system (which is orthogonal and diffractometer-specific), and the ϕ-axis system, also orthogonal, which is attached rigidly to the ϕ circle of the diffractometer and coincides with the laboratory system when all diffractometer circles are at zero. The unit vector in the ϕ-axis system corresponding to the short axis of the pressure cell, $\boldsymbol{p}_\phi$, can be written

$$\begin{pmatrix} 0 \\ 1 \\ 0 \end{pmatrix}$$

if it coincides with the diffractometer y-axis when all circles are at zero, although this setting may be hypothetical on fixed-chi instruments, such as the SMART. In order to derive the absorption correction the angle made by this vector with the incident and diffracted beams is required. It is convenient to perform these corrections using a file containing intensities corrected for Lp and other geometric effects such as air absorption. Consider a reflection in which the diffracted-beam has direction cosines m_1, m_2 and m_3 with the reciprocal cell axes a^*, b^* and c^*, respectively. A unit vector, $\boldsymbol{d}$, representing the direction of the diffracted beam in the reciprocal axis system is given by $d_1\boldsymbol{a}^* + d_2\boldsymbol{b}^* + d_3\boldsymbol{c}^*$. By definition

$$\boldsymbol{G}^*\boldsymbol{d}_r = \boldsymbol{m}$$

where $\boldsymbol{G}^*$ is the reciprocal metric tensor

$$\boldsymbol{m} = \begin{pmatrix} m_1 a* \\ m_2 b* \\ m_3 c* \end{pmatrix}$$

and

$$\boldsymbol{d}_r = \begin{pmatrix} d_1 \\ d_2 \\ d_3 \end{pmatrix}.$$

Hence

$$\boldsymbol{d}_r = \boldsymbol{G}\boldsymbol{m}$$

where $\boldsymbol{G}$ is the metric tensor ($\boldsymbol{G}^* = \boldsymbol{G}^{-1}$). This vector is transformed from the reciprocal axis system into the ϕ-axis system with the orientation matrix, $\boldsymbol{A}$ (which corresponds to Busing and Levy's matrix product, $\boldsymbol{UB}$):

$$\boldsymbol{d}_\phi = \boldsymbol{A}\boldsymbol{d}_r = \boldsymbol{A}\boldsymbol{G}\boldsymbol{m} = \boldsymbol{A}(\boldsymbol{A}^T\boldsymbol{A})^{-1}\boldsymbol{m} = (\boldsymbol{A}^T)^{-1}\boldsymbol{m}$$

where $\boldsymbol{A}^T$ is the transpose of $\boldsymbol{A}$. The cosine of the angle between the cell axis and the diffracted beam is $\boldsymbol{d}_\phi \cdot \boldsymbol{p}_\phi$ (both $\boldsymbol{d}$ and $\boldsymbol{p}$ being unit vectors). The angle made with the reverse incident beam is calculated in a similar manner. If either the diffracted or incident beam makes an angle of greater than 40° with $\boldsymbol{p}_\phi$ then the beam is completely absorbed by the cell and the detector shaded. These data were omitted; also omitted were data with very poorly-fitting profiles.

The surviving reflections were corrected for absorption by the pressure cell components with the program SADABS. The transmission ranged from 0.525 to 1.000. The low minimum transmission factor arises because of partial shadowing by the highly-absorbing tungsten gasket, which is difficult to model analytically. A least-squares refinement was performed against F^2 in which all four molecules were restrained to have similar 1,2 and 1,3 distances, H-atoms were placed in calculated positions and all non-H atoms were refined with isotropic displacement parameters (Shelxl97) [7]. The final residuals were $R1 = 8.23\%$ based on F and 314 unique data with $F > 4\sigma(F)$ and $a\ wR2 = 26.26\%$ based on F^2 and all 631 data used for refinement of 82 parameters. The goodness-of-fit was 0.998 and the completeness of the data set was 29%. These parameters constitute a considerable improvement over the refinements obtained from the CAD4 data. The unit cell was found to be $a = 7.505(7)$ Å, $b = 7.614(7)$ Å, $c = 14.219(14)$ Å, $\alpha = 101.47(2)^\circ$, $\beta = 103.80(2)^\circ$ and $\gamma = 99.109(14)^\circ$ with a volume $V = 755.0(12)$ Å^3 and the structural parameters are presented in table 1.

A further loading of the Merrill–Bassett cell (using both a new gasket and sample) gave a quite different behaviour. Following the same experimental procedure as before (using the CAD4 diffractometer), the low-temperature monoclinic phase was found to be stable at a pressure of 0.9 GPa with cell dimensions of $a = 3.8748(13)$ Å, $b = 8.8152(19)$ Å, $c = 10.749(3)$ Åand $\beta = 90.00(2)^\circ$ with a volume $V = 367.2(3)$ Å^3. The initial model was taken from the structure reported by Frederick *et al* [5] and the final structural parameters to the fit ($R1 = 12.15\%$ for 136 unique data with $F > 4\sigma(F)$ and $a\ wR2 = 32.84\%$ based on F^2 and all 255 data used for refinement, goodness-of-fit = 1.218) are presented in table 2.

To obtain a better understanding of the nature of the phases found experimentally, we have performed a series of *ab initio* calculations using the CASTEP code [8]. This also allows us to obtain accurate hydrogen positions which are extremely difficult to obtain experimentally. Calculations were performed within the density functional formalism using the generalized gradient approximation [9] to treat the many-body effects of electron exchange and correlation. Vanderbilt ultrasoft pseudopotentials [10] are used to describe the valence electron–ionic core interactions. The electronic wavefunction is expanded in a plane-wave basis set up to a kinetic energy of 500 eV which we find converges the total energy of the system to better than 1m eV/atom. Brillouin zone integrations are performed by using a Monkhorst–Pack [11] k-point set. In each calculation presented here, a k-point density is chosen so that the total energy of the system is also better than 1 meV/atom. The electronic structure is optimized by use of a conjugate gradients energy minimization scheme. The positions of the atoms within the unit cell are optimized also using a conjugate gradients method and the *ab initio* Hellmann–Feynman forces. In conjunction with this, the unit cell parameters are optimized using the calculated stresses. For this, a finite basis set correction is employed to compensate for the changing basis set (plane wave kinetic energies) as the lattice parameters change throughout the course of the energy minimization. However, we have chosen the basis set cutoff energy high enough such that this basis set correction is extremely small. In tables 1 and 2, we show the free atomic positional parameters obtained for each structure, both experimentally and theoretically and it can be seen that the experimental and theoretical values are in good agreement. The calculated unit cell dimensions are also in good agreement: for the triclinic phase we obtain $a = 7.4766$ Å, $b = 7.6232$ Å, $c = 13.9353$ Å, $\alpha = 102.6511^\circ$, $\beta = 101.4290^\circ$ and $\gamma = 98.1514^\circ$; and for the monoclinic phase we get $a = 4.0306$ Å, $b = 8.8992$ Å, $c = 10.8373$ Åand $\beta = 88.287^\circ$.

Table 1. Fractional co-ordinates ($\times 10^4$) of the high-pressure triclinic, $P\bar{1}$, propionic acid structure obtained from the *ab initio* calculations (second set of co-ordinates) and, for comparison, the co-ordinates obtained from the SMART single-crystal x-ray diffraction results (first set). The standard deviations from the single-crystal refinements are shown in parenthesis.

	Experimental			Theoretical		
	x	y	z	x	y	z
O1A	2989(14)	3059(11)	−2178(11)	3001	3160	−2102
O2A	4373(14)	4508(12)	−3099(12)	4372	4606	−3008
H2A	3529	5067	−3081	3376	5361	−2975
C1A	4240(20)	3250(20)	−2591(17)	4200	3334	−2537
C2A	5710(20)	2157(19)	−2540(18)	5539	2122	−2591
H2A1	5700	1592	−3215	5229	1466	−3384
H2A2	6922	2981	−2217	6905	2943	−2388
C3A	5490(20)	709(18)	−2000(17)	5485	770	−1976
H3A1	5636	1261	−1309	5932	1394	−1182
H3A2	6425	−2	−2049	6404	−152	−2113
H3A3	4261	−76	−2289	4110	−6	−2157
O1B	1819(15)	6570(12)	−2953(12)	1913	6649	−2928
O2B	430(16)	5016(13)	−2072(13)	595	5174	−2014
H2B	1214	4401	−2144	1573	4391	−2072
C1B	710(20)	6430(18)	−2455(17)	738	6451	−2478
C2B	−650(20)	7638(18)	−2385(17)	−644	7629	−2416
H2B1	−1912	6883	−2636	−2002	6771	−2712
H2B2	−457	8221	−1686	−499	8138	−1622
C3B	−510(20)	9073(18)	−2935(17)	−520	9120	−2915
H3B1	719	9312	−3031	−246	9541	−2936
H3B2	−728	10176	−2561	−757	10073	−2590
H3B3	−1437	8670	−3574	−602	8619	−3716
O1C	2140(12)	−233(10)	5362(10)	2168	−173	5367
O2C	−294(13)	−2469(12)	4457(10)	−227	−2324	4482
H2C	−856	−1633	4526	−959	−1309	4546
C1C	1497(14)	−1844(13)	4933(12)	1533	−1746	4926
C2C	2654(16)	−3251(13)	4871(14)	2693	−3141	4841
H2C1	2122	−4253	5117	2073	−4255	5082
H2C2	2571	−3738	4174	2522	−3648	4043
C3C	4642(17)	−2590(16)	5429(15)	4689	−2506	5413
H3C1	5178	−1574	5206	5308	−1408	5167
H3C2	5299	−3562	5319	5470	−3567	5310
H3C3	4750	−2201	6129	4858	−2059	6210
O1D	−2181(13)	−4831(10)	−406(10)	−2197	−4900	−423
O2D	236(13)	−2557(12)	417(10)	185	−2709	437
H2D	795	−3399	366	952	−3712	418
C1D	−1564(14)	−3204(13)	−15(12)	−1567	−3310	−13
C2D	−2751(16)	−1821(13)	−2(14)	−2725	−1912	22
H2D1	−2699	−1294	687	−2571	−1383	815
H2D2	−2220	−840	−263	−2084	−825	−231
C3D	−4734(17)	−2529(17)	−578(14)	−4713	−2551	−559
H3D1	−4812	−2974	−1271	−4863	−3079	−1347
H3D2	−5408	−1562	−506	−5477	−1463	−510
H3D3	−5274	−3513	−333	−5362	−3587	−281

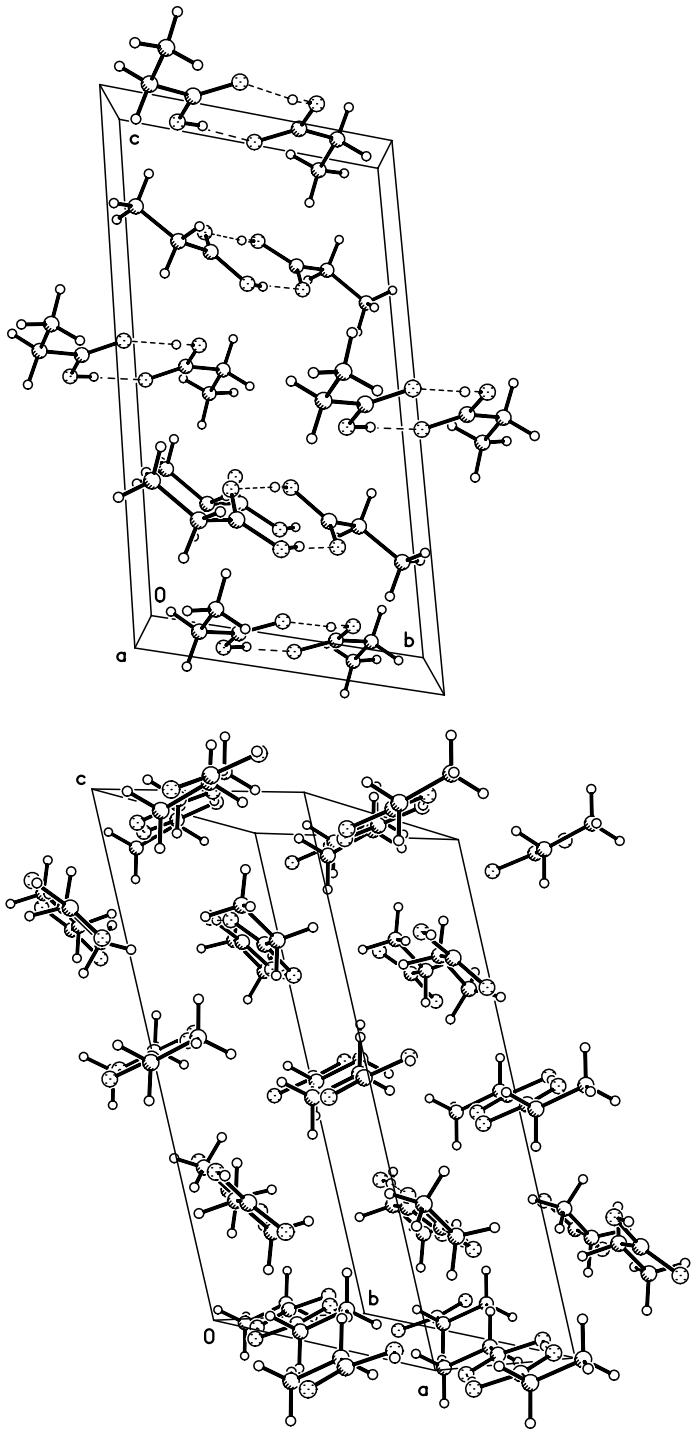

Figure 1. The crystal structure of the high-pressure triclinic, $P\bar{1}$, phase of propionic acid viewed (top) approximately down the *a*-axis of the unit cell and (bottom) along a direction showing the herringbone packing motif of the molecules.

Table 2. Fractional co-ordinates ($\times 10^4$) of the high-pressure monoclinic, $P2_1/c$, propionic acid structure obtained from the *ab initio* calculations (second set of co-ordinates) and, for comparison, the co-ordinates obtained from the CAD4 single-crystal x-ray diffraction results (first set). The standard deviations from the single-crystal refinements are shown in parenthesis.

	Experimental			Theoretical		
	x	y	z	x	y	z
O1	7256(38)	−282(10)	1257(8)	7192	−287	1277
O2	4776(21)	1831(6)	685(6)	4849	1870	741
H1	4318	1299	81	4024	1236	34
C1	6683(21)	1056(6)	1471(6)	6527	1042	1513
C2	7742(21)	1857(6)	2620(6)	7367	1810	2689
H2	9482	2606	2411	8871	2812	2490
H3	5764	2392	2957	5033	2227	3105
C3	9140(21)	831(6)	3586(6)	9073	751	3540
H4	7278	292	3976	7503	−217	3745
H5	10350	1416	4200	9618	1325	4390
H6	10699	120	3210	11382	355	3108

Perhaps the most striking feature of the high-pressure $P\bar{1}$ phase of propionic acid is the herringbone packing arrangement of the molecules (see figure 1). This differs markedly from the essentially flat dimer-stacking of the $P2_1/c$ phase of propionic acid and the low-temperature phases of the heavier members of the monocarboxylic acid series: e.g. butyric acid (C_3H_7COOH, C2/m) [12] and valeric acid (C_4H_9COOH, $P2_1/c$) [13]. We have observed a similar structural difference in acetic acid [2] where the low-temperature orthorhombic, $Pna2_1$, structure is composed of catemers (molecular chains) adopting an essentially herringbone packing arrangement while the high-pressure monoclinic, $P2_1/n$, structure has catemers adopting planar stacking—the catemers themselves are basically unaffected by the change in packing arrangement. This rearrangement of neighbouring catemers is accompanied by a more efficient molecular packing: in the low-temperature structure, at 287 K, each molecule occupies a volume of 78.51 Å^3 while at high pressure the molecular volume is 75.99 Å^3. Similarly, the rearrangement of the dimers in the high-pressure $P\bar{1}$ phase of propionic acid gains a more efficient molecular packing with respect to that observed in the $P2_1/c$ phase although the improvement is only marginal: each molecule occupies 90.01 Å^3 rather than 91.79 Å^3. From *ab initio* pseudo-potential calculations, we find that for acetic acid there is a relatively small, 0.056 eV/molecule, enthalpy difference between the two structures and indicates that they have similar stabilities. For propionic acid, the calculations reveal that the herringbone arrangement of the molecules results in a decrease of the enthalpy but by only 0.062 eV/molecule. Compared to a room temperature k_BT of 2.5 meV, this relatively small energy difference, coupled with the slight improvement in molecular packing efficiency, may explain why the monoclinic and triclinic phases can occur in the same narrow pressure range just above the ambient temperature crystallization pressure.

Finally, it is interesting to note that the reduction of symmetry from monoclinic $P2_1/c$ to triclinic $P\bar{1}$ has the consequence that one of the dimers, containing molecules A and B, is not centred on a point of inversion. However, by placing a pseudo inversion centre at (0.2476, 0.4859, −0.2500) we note that the maximum displacement of molecules A and B from this ideal symmetry is only 0.10 Å for the C3A and C3B and hence the three crystallographically unique dimers within the structure can be considered to be essentially identical. The program MISSYM[94] was used to confirm that no symmetry has been missed in the model presented.

In conclusion, we have solved the high-pressure triclinic P crystal structure of propionic

acid and find that both this previously unobserved phase and the low-temperature monoclinic $P2_1/c$ phase are both stable over a narrow region of pressure just above that of the onset of crystallization. The dimer pairs of molecules in the triclinic phase arrange themselves in a herringbone packing motif which is strikingly different from the planar arrangement of the monoclinic form and results in two different classes of dimers—depending on whether or not the dimers are located on centres of inversion. This rearrangement of the molecules results in a very small reduction in the enthalpy (0.062 eV/molecule) for the triclinic structure and may explain why both the monoclinic and triclinic phases can crystallize from the melt at much the same pressure.

This study also demonstrates the use of an area detector diffractometer for collecting very high quality diffraction data from a single-crystal sample contained within a diamond anvil cell. Although the data sets are not identical, it is nevertheless instructive to compare the area-detctor and point-detector refinements. For the point-detector, the number of observed reflections, $F > 4\sigma(F)$, is only 35% of the total number collected and this contrasts markedly with the area-detector data where a total of 74% are observed. The statistical parameters of the fit to the area-detector data also show a substantial improvement over those obtained from the single-detector data (e.g. R1 decreases from 18.68% to 6.98%) though the data collection time was much reduced from about a week to only a few hours. The significant improvement in the quality of the intensity data is also reflected in the increased precision of the refined structural parameters. In addition, as the ratio of observed to unobserved reflections and the statistics of the fit have improved dramatically, the refined structural parameters are expected to be more accurate. As area detector diffractometers are coming to particular prominence for ambient-pressure single-crystal diffraction, where they will eventually supplant conventional point-detector methods, the high-pressure single-crystal diffraction techniques described here will need to be further developed to optimize the benefits that these new machines provide for accurate, and rapid, integrated intensity measurements.

We thank H Vass for his help in maintaining and preparing the x-ray diffraction facilities. This work is supported by a grant from the Engineering and Physical Sciences Research Council.

References

[1] Allan D R and Clark S J 1999 *Phys. Rev. Lett.* **82** 3464
[2] Allan D R and Clark S J 1999 *Phys. Rev.* B 60 6328
[3] Merrill L and Bassett W A 1974 *Rev. Sci. Instrum.* **45** 290
[4] Vos W L *et al* 1992 *Nature* **358** 46
Vos W L *et al* 1993 *Phys. Rev. Lett.* **71** 3150
[5] Frederick J S, Templeton D H, Scheuerman R F and Sass R L 1962 *Acta. Crystalolgr.* **15** 1233
[6] Finger L W and King H 1978 *Am. Mineral.* **63** 337
[7] Sheldrick G M, 1997 Shelxl-97, University of Göttingen
[8] Payne M C, Teter M P, Allan D C, Arias T A, Joannopolous J 1992 *Rev. Mod. Phys.* **64** 1045; CASTEP 4.2, academic version, licensed under the UKCP-MSI agreement (1999)
[9] Perdew J P and Wang Y 1992 *Phys. Rev.* B **46** 6671
[10] Monkhorst J H and Pack J D 1976 *Phys. Rev.* B **13** 5188
[11] Vanderbilt D 1990 *Phys. Rev.* B **41** 7892
[12] Strieter F J and Templeton D H 1962 *Acta. Crystallogr.* **15** 1240
[13] Scheureman R F and Sass R L 1962 *Acta Crystallogr.* **15** 1244
[14] Le Fuge Y 1987 *J. Appl. Crystallogr.* **20** 264
Spek A L 1990 *Acta Crystallogr.* A **46** C34